BRAIN
A JOURNAL OF NEUROLOGY

Earliest amyloid and tau deposition modulate the influence of limbic networks during closed-loop hippocampal downregulation

Stavros Skouras,[1,*] Jordi Torner,[2] Patrik Andersson,[3] Yury Koush,[4] Carles Falcon,[1,5,6] Carolina Minguillon,[1,6,7] Karine Fauria,[1,7] Francesc Alpiste,[2] Kaj Blenow,[8,9] Henrik Zetterberg,[8,9,10,11] Juan D. Gispert[1,5,6,12] and José L. Molinuevo[1,6,7,12] on behalf of the ALFA Study[#]

[#]Appendix 1.

See Agosta *et al.* (doi:10.1093/brain/awaa038) for a scientific commentary on this article.

Research into hippocampal self-regulation abilities may help determine the clinical significance of hippocampal hyperactivity throughout the pathophysiological continuum of Alzheimer's disease. In this study, we aimed to identify the effects of amyloid-β peptide 42 (amyloid-β_{42}) and phosphorylated tau on the patterns of functional connectomics involved in hippocampal downregulation. We identified 48 cognitively unimpaired participants (22 with elevated CSF amyloid-β peptide 42 levels, 15 with elevated CSF phosphorylated tau levels, mean age of 62.705 ± 4.628 years), from the population-based 'Alzheimer's and Families' study, with baseline MRI, CSF biomarkers, *APOE* genotyping and neuropsychological evaluation. We developed a closed-loop, real-time functional MRI neurofeedback task with virtual reality and tailored it for training downregulation of hippocampal subfield cornu ammonis 1 (CA1). Neurofeedback performance score, cognitive reserve score, hippocampal volume, number of apolipoprotein ε4 alleles and sex were controlled for as confounds in all cross-sectional analyses. First, using voxel-wise multiple regression analysis and controlling for CSF biomarkers, we identified the effect of healthy ageing on eigenvector centrality, a measure of each voxel's overall influence based on iterative whole-brain connectomics, during hippocampal CA1 downregulation. Then, controlling for age, we identified the effects of abnormal CSF amyloid-β_{42} and phosphorylated tau levels on eigenvector centrality during hippocampal CA1 downregulation. Across subjects, our main findings during hippocampal downregulation were: (i) in the absence of abnormal biomarkers, age correlated with eigenvector centrality negatively in the insula and midcingulate cortex, and positively in the inferior temporal gyrus; (ii) abnormal CSF amyloid-β_{42} (<1098) correlated negatively with eigenvector centrality in the anterior cingulate cortex and primary motor cortex; and (iii) abnormal CSF phosphorylated tau levels (>19.2) correlated with eigenvector centrality positively in the ventral striatum, anterior cingulate and somatosensory cortex, and negatively in the precuneus and orbitofrontal cortex. During resting state functional MRI, similar eigenvector centrality patterns in the cingulate had previously been associated to CSF biomarkers in mild cognitive impairment and dementia patients. Using the developed closed-loop paradigm, we observed such patterns, which are characteristic of advanced disease stages, during a much earlier presymptomatic phase. In the absence of CSF biomarkers, our non-invasive, interactive, adaptive and gamified neuroimaging procedure may provide important information for clinical prognosis and monitoring of therapeutic efficacy. We have released the developed paradigm and analysis pipeline as open-source software to facilitate replication studies.

1 Barcelonaβeta Brain Research Center (BBRC), Pasqual Maragall Foundation, Barcelona, Spain
2 BarcelonaTech, Universitat Politècnica de Catalunya (UPC), Barcelona, Spain
3 SUBIC, Stockholm University, Stockholm, Sweden
4 Department of Radiology and Biomedical Imaging, Yale University, New Haven, CT, USA

5 Centro de Investigación Biomédica en Red de Bioingeniería, Biomateriales y Nanomedicina (CIBER-BBN), Madrid, Spain
6 IMIM (Hospital del Mar Medical Research Institute), Barcelona, Spain
7 CIBER Fragilidad y Envejecimiento Saludable (CIBERFES), Madrid, Spain
8 Department of Psychiatry and Neurochemistry, Institute of Neuroscience and Physiology, The Sahlgrenska Academy at University of Gothenburg, Mölndal, Sweden
9 Clinical Neurochemistry Laboratory, Sahlgrenska University Hospital, Mölndal, Sweden
10 Department of Neurodegenerative Disease, UCL Institute of Neurology, Queen Square, London, UK
11 UK Dementia Research Institute at UCL, University College London, London, UK
12 Universitat Pompeu Fabra, Barcelona, Spain

*Present address: Department of Biological and Medical Psychology, University of Bergen, Bergen, Norway

Correspondence to: José Luis Molinuevo Guix
Scientific Director, Alzheimer Prevention Program, Barcelonaβeta Brain Research Center
Wellington 30, 08005, Barcelona, Spain
E-mail: jlmolinuevo@barcelonabeta.org

Introduction

Alzheimer's disease poses a global threat to millions of lives and the sustainability of public healthcare (Prince *et al.*, 2015). Recent progress is shifting the mainstream dual clinic-pathological concept of Alzheimer's disease towards a pathophysiological 'continuum', with progression being monitored *in vivo* through the study of CSF and PET biomarkers (Jack *et al.*, 2018). The study of the brain alterations associated with the presence of abnormal levels of biomarkers in unimpaired individuals may shed light on factors and mechanisms associated with cerebral resilience or vulnerability to early Alzheimer's disease pathology.

According to the 'compensation-related utilization of neural circuits hypothesis' (CRUNCH; Reuter-Lorenz and Cappell, 2008) and the 'network-based degeneration' theory (Seeley *et al.*, 2009), functional alterations such as hippocampal hyperactivity during the preclinical stage are likely to be initially compensated by specific changes in functional connectomics (Jacobs *et al.*, 2013). In network science, eigenvector centrality (EC) is one of the most advanced connectomic metrics (Bonacich, 1972; Langville and Meyer, 2006) that is designed to reflect the influence of each node on the overall connectomic patterns of a network (Borgatti, 2005; Lohmann *et al.*, 2010; Wink *et al.*, 2012). For example, when applied to social interactions, EC can determine the members of a social network exerting the most influence (Bonacich, 1972) and EC is also the metric subserving the most successful internet search engine (Langville and Meyer, 2006). In functional neuroimaging, eigenvector centrality mapping (ECM) is an assumption-free, data-driven procedure that can be performed in high image resolution, for each participant, using the time series from every individual voxel while accounting for global brain patterns of functional connectivity. ECM derives estimates of relative influence on whole

brain connectomics, per voxel or cluster of voxels (Lohmann *et al.*, 2010; Wink *et al.*, 2012). Importantly, EC values can be processed to meet parametric assumptions, enabling group-level regression with biomarker covariates to be performed. These features make ECM particularly promising for the investigation of changes along disease continuums such as the pathophysiological continuum of Alzheimer's disease (Skouras *et al.*, 2019a).

Previous studies have shown that EC reveals similar patterns to fluorodeoxyglucose (FDG)-PET when comparing patients with Alzheimer's disease to healthy controls (Adriaanse *et al.*, 2016), and that patients with Alzheimer's disease present significant differences in EC, in the anterior cingulate cortex (ACC), paracingulate gyrus, cuneus and occipital cortex (Binnewijzend *et al.*, 2014). An independent study found that increased EC in the cingulate cortex and thalamus is related to compensatory mechanisms across the pathophysiological continuum of Alzheimer's disease, and evidenced a relation of these EC patterns to reduced functional connectivity between the midcingulate cortex and the left hippocampus during the preclinical phase of Alzheimer's disease (Skouras *et al.*, 2019a). The latter finding suggested that EC changes may comprise a sensitive indicator of preclinical changes in functional connectomics related to hippocampal function. However, all previous investigations of EC in Alzheimer's disease have been limited to task-free (i.e. resting state) functional MRI, even though EC is particularly suited for the explorative investigation of differences in task-related connectivity with functional MRI designs featuring long, continuous experimental conditions (Koelsch and Skouras, 2014; Alnæs *et al.*, 2015). Recent evidence suggests that functional tasks that engage specific brain regions affected by a disease lead to stronger effects and consequently to higher discriminative power between patients and controls (Finn *et al.*, 2017; Greene *et al.*, 2018). In the present study, we aimed to investigate preclinical differences of EC related

to hippocampal function, by harnessing the sensitivity of CSF biomarkers.

Across Alzheimer's disease patient studies and healthy memory studies, the hippocampus has been established to be the single brain region with the most important role (Schwindt and Black, 2009; Kim, 2011). Hippocampal subfield CA1 in particular, appears to be a region that is integral to contextual episodic memory (Mizumori *et al.*, 1999; Leutgeb *et al.*, 2004; Vazdarjanova and Guzowski, 2004; Penner and Mizumori, 2012). CA1 presents atrophy linked to Alzheimer's disease pathology but no volume loss related to normal ageing (Wilson *et al.*, 2004; Frisoni *et al.*, 2008; Yushkevich *et al.*, 2015). Here, we focus on hippocampal subfield CA1 because we reasoned that if preclinical alterations in brain function indeed occur prior to neurodegeneration as has been suggested (Pihlajamäki and Sperling, 2008; Teipel *et al.*, 2015), it is probable that they are most prominent in areas that later undergo atrophy due to Alzheimer's disease. Hippocampal hyperactivity appears to precede amyloid accumulation (Leal *et al.*, 2017), which is accepted as the earliest sign of preclinical Alzheimer's disease (Jack *et al.*, 2018). Hippocampal hyperactivity also appears to be more prominent in subjects at genetic risk for Alzheimer's disease (Tran *et al.*, 2017). The lack of concurrent neurodegeneration or decline in cognitive performance (Leal *et al.*, 2017; Tran *et al.*, 2017) implies: (i) that hippocampal hyperactivity is the result of compromised neural efficiency, as defined in the context of neural reserve (Barulli and Stern, 2013; Stern *et al.*, 2018); and (ii) a potential link between hippocampal hyperactivity and compromised hippocampal downregulation abilities. In this context, developing a standard framework for the investigation of the ability to downregulate hippocampal activation may bring us a step closer to detecting Alzheimer's disease-specific signs earlier along the pathophysiological continuum of Alzheimer's disease.

Real-time neurofeedback enables focusing investigations on specific brain regions and their self-regulation during interactive functional tasks (Sitaram *et al.*, 2017). Neurofeedback with real-time functional MRI (rt-fMRI) is particularly suited to study hippocampal downregulation due to the spatiotemporal resolution of functional MRI and the deep-brain location of the hippocampus. In a previous rt-fMRI neurofeedback study of healthy young adults, memory performance correlated with downregulation, but not upregulation, of the parahippocampal formation (Weiskopf *et al.*, 2004). Moreover, a recent study has demonstrated that rt-fMRI neurofeedback is suitable for the downregulation of deep-brain structures (e.g. the amygdala that is adjacent to the hippocampus), as well as a link between amygdala downregulation and clinical symptoms (Nicholson *et al.*, 2017). In addition, neurofeedback tasks can be combined with virtual reality (VR). VR has shown promise for the development of immersive experimental tasks with increased ecological validity (Krokos *et al.*, 2018), which have revealed significant insights regarding hippocampal function (Duarte *et al.*, 2014; Igloi *et al.*, 2014; Dimsdale-Zucker *et al.*, 2018). Furthermore, VR promotes participants' experimental compliance, through perceptual immersion in engaging tasks (Chirico *et al.*, 2017) that in turn can result in higher engagement (Torner *et al.*, 2019) and improved performance (Krokos *et al.*, 2018). The increased engagement and compliance afforded by VR tasks, facilitates focused participation in long functional tasks. Combined with closed-loop neurofeedback paradigms, long tasks enable the acquisition of continuous whole-brain datasets that are optimal for the reliable estimation of functional connectomics (Gonzalez-Castillo *et al.*, 2014; Finn *et al.*, 2015), including EC.

Here, we fused state-of-the-art, disruptive technologies (i.e. fully automated electrochemiluminescence immunoassay, real-time functional neuroimaging and VR), aiming to create an interactive and entertaining task to investigate the neural correlates of hippocampal downregulation, associated with core Alzheimer's disease CSF biomarkers and healthy ageing, in a sample of cognitively unimpaired participants at risk for Alzheimer's disease. We hypothesized that: (i) to downregulate hippocampal activation, participants with hippocampal hyperactivity engage their brain differently or more strongly than healthy agers and that such differences can be captured by EC during hippocampal downregulation; and (ii) we may identify patterns of functional connectomics during hippocampal downregulation that resemble those found during resting state at advanced Alzheimer's disease stages. Specifically, we expected to find measurable differences of EC in the occipital cortex (Binnewijzend *et al.*, 2014), the inferior parietal lobule, the thalamus and the cingulate cortex (Binnewijzend *et al.*, 2014; Skouras *et al.*, 2019a).

Materials and methods

Participants

Participants comprised 48 adult volunteers with complete data [mean age = 62.705 years; standard deviation (SD) = 4.628] from the ongoing ALFA (Alzheimer's and Families) project and related substudies, many of them descendants of patients with Alzheimer's disease and *APOE* ε4 allele carriers, hence presenting increased risk for Alzheimer's disease (Molinuevo *et al.*, 2016). All data were acquired at the Barcelonaβeta Brain Research Center, from 2016–18. Researchers were blind to biomarker levels and cognitive performance during data acquisition. All participants were highly functional and without neurological or psychiatric history at the time of scanning, as assessed in the medical baseline session of their ongoing ALFA-related study within the previous 12 months (time between baseline ALFA and rt-fMRI scanning: mean = 6.4 months, SD = 2.5). The cognitively unimpaired status of participants was also assessed as an inclusion criterion in the cognitive testing session of their ongoing ALFA-related study within the previous 12 months (mean = 6.4 months, SD = 2.5), according to their scores on the Clinical Dementia Rating scale (CDR = 0; Hughes *et al.*,

1982; Morris, 1993) and the Mini-Mental State Examination (MMSE $\geqslant$ 27; Folstein *et al.*, 1975; Blesa *et al.*, 2001). During that cognitive testing session, participants also completed the Free and Cued Selective Reminding Test (FCSRT; Grober *et al.*, 2009), the Subjective Cognitive Decline Questionnaire (SCD-Q; Rami *et al.*, 2014) and the Visual Puzzles test included in the Wechsler Adult Intelligence Scale IV (WAIS IV; Weschler, 2013); all scores are summarized in Table 1. The FCSRT is an internationally standardized research instrument recommended for the assessment of episodic memory and diagnosis of prodromal Alzheimer's disease (Dubois *et al.*, 2007, 2014). The SCD-Q is a useful tool to measure self-perceived cognitive decline, independently of a participant's objective neuropsychological assessment. According to their SCD-Q responses, four participants had a subjective impression of cognitive or memory decline, while their cognition was preserved based on objective cognitive testing (see 'Discussion' section). The Visual Puzzles test measures non-verbal reasoning and the ability to analyse and synthesize abstract visual stimuli. It is related to visual perception, general visuospatial intelligence, fluid intelligence, simultaneous processing, visualization and spatial manipulation, as well as the ability to anticipate relationships between constituent parts of a whole. Within a given time limit (either 20 or 30 s, depending on the complexity of a puzzle), the participant was instructed to select the three pieces necessary for the reconstruction of the presented puzzle. Each item is scored with 0 or 1 and the testing is suspended after three consecutive scores of 0. The test consists of 26 items and the estimated administration time is ~10 min. At inclusion of participants in the ALFA project, they had also completed the Cognitive Reserve Questionnaire (CRQ; Supplementary Table 1); a questionnaire comprising eight questions whose total score serves as a proxy for cognitive reserve (Rami *et al.*, 2011). To assess core Alzheimer's disease biomarker levels in CSF, participants underwent lumbar puncture within the preceding 10 months (time between lumbar puncture and rt-fMRI scanning: mean = 5.23 months, SD = 2.49). Eighteen participants presented normal CSF biomarkers (amyloid-β_{42} levels > 1098 pg/ml and p-tau levels < 19.2 pg/ml), 22 participants presented CSF amyloid-β_{42} levels < 1098 pg/ml, 15 participants presented CSF p-tau levels > 19.2 pg/ml and seven of the latter met both criteria. Participants did not differ significantly with regards to any cognitive or neuroimaging variables, regardless of grouping based on CSF amyloid-β_{42} and p-tau levels (Table 1). Thorough quality control was applied in advance, to exclude five datasets with >10% invalid functional volumes due to movement, as well as seven datasets with rt-fMRI acquisitions during which technological complications occurred and six datasets with rt-fMRI acquisitions during which fatigue, discomfort or sleep had occurred. The local ethics committee 'CEIC-Parc de Salut Mar' reviewed and approved the study protocol and informed consent form, in accordance with current legislation.

CSF sampling

CSF was collected by lumbar puncture between 9 and 12 am in polypropylene tubes. Samples were processed within 1 h and centrifuged at 4°C for 10 min at 2000*g*, stored in polypropylene tubes and frozen at –80°C. Core Alzheimer's disease CSF biomarkers (namely amyloid-β_{42} and p-tau) were determined using cobas Elecsys® assays (Hansson *et al.*, 2018).

APOE genotyping

Proteinase K digestion and subsequent alcohol precipitation was used to obtain DNA from the blood cellular fraction. Samples were genotyped for two single nucleotide polymorphisms (rs429358 and rs7412) and the number of *APOE* ε4 alleles was determined for each participant (Molinuevo *et al.*, 2016). Results are displayed in Table 2.

Image acquisition

All scanning was performed in a single 3 T Philips Ingenia CX MRI scanner (2015 model). Pre-neurofeedback scanning comprised a 3D T_1-weighted sequence of 240 sagittal slices with voxel resolution = $0.75 \times 0.75 \times 0.75$ mm^3, repetition time = 9.90 ms, echo time = 4.60 ms, flip angle = 8; and a diffusion-weighted sequence of 66 axial slices with voxel resolution = $2.05 \times 2.05 \times 2.20$ mm^3, repetition time = 9000 ms, echo time = 90 ms, flip angle = 90, featuring 72 non-collinear directions (b = 1300 s/mm^2) and one non-gradient volume (b = 0 s/mm^2). During neurofeedback, echo planar imaging was used with voxel resolution = $3 \times 3 \times 3$ mm^3, repetition time = 3000 ms, echo time = 35 ms, matrix size = 80×80 voxels, field of view = 240 mm and interleaved slice acquisition with an interslice gap of 0.2 mm (45 slices, whole brain coverage). In total, 610 functional volumes were acquired.

Structural image processing

The standard FreeSurfer pipeline was applied on T_1-weighted images to estimate each participant's normalized hippocampal brain volume, as a proxy of brain reserve, by dividing total hippocampal volume by total intracranial volume (Cavedo *et al.*, 2012). Using the Advanced Normalization Tools (Avants *et al.*, 2009) (ANTs v2.x; RRID: SCR_004757), the N4 non-parametric non-uniform intensity normalization bias correction function (Tustison *et al.*, 2010; Tustison and Avants, 2013) was applied on all T_1 images, followed by an optimized blockwise non-local means denoising filter (Coupé *et al.*, 2008). Multi-atlas segmentation with joint label fusion (Wang *et al.*, 2013) segmented hippocampal subfields to derive probabilistic maps for CA1, which were thresholded at $P = 0.9$ to create the neurofeedback target region of interest masks.

Experimental paradigm

The design of the VR paradigm was guided by the following objectives: (i) we used VR to make the task immersive, engaging and entertaining, which in turn; (ii) enabled us to extend the task to 30 min to maximize first-level statistical power; (iii) we used sliding-window closed-loop neurofeedback to achieve an optimal design for analysis of functional connectomics; and (iv) we narrowed the neurofeedback target region of interest to hippocampal subfield CA1, which presents atrophy in Alzheimer's disease but not in healthy ageing (Wilson *et al.*, 2004; Frisoni *et al.*, 2008; Yushkevich *et al.*, 2015), while also being consistently implicated in memory encoding (Kim, 2011) and differing in activity in patients (Schwindt and Black, 2009). Prior to the acquisition of CSF biomarkers, the task

Table 1 Descriptive and comparative statistics, across groupings based on CSF amyloid-β_{42} and p-tau levels

	Entire sample Mean (SD)	Controls	Amyloid-β_{42} < 1098 Mean (SD)	p-tau > 19.2 Mean (SD)	PreAD Mean (SD)
n; M / F	48; 21 / 27	18; 7 / 11	22; 10 / 12	15; 8 / 7	7; 4 / 3
Age	62.705 (4.628)	62.143 (4.690)	62.143 (5.171) $t = -0.099$ $P = 0.921$	65.051 (2.306) $t = 2.070$ $P = 0.046^*$	64.919 (3.202) $t = 1.352$ $P = 0.193$
Aβ42	1186.200 (424.678)	1492.111 (232.529)	795.123 (232.529) $t = -9.677$ $P < 0.001^{***}$	1189.60 (454.94) $t = -2.423$ $P = 0.022^*$	771.06 (190.47) $t = -7.636$ $P < 0.001^{***}$
p-Tau	18.233 (9.007)	14.735 (3.046)	16.645 (8.190) $t = 0.936$ $P = 0.367$	28.624 (8.819) $t = 6.265$ $P < 0.001^{***}$	26.513 (6.554) $t = 6.221$ $P < 0.001^{***}$
t-Tau	220.273 (86.623)	1.906 (37.090)	1984.318 (73.441) $t = 0.410$ $P = 0.687$	318.133 (81.981) $t = 5.925$ $P < 0.001^{***}$	285.071 (55.774) $t = 4.959$ $P < 0.001^{***}$
p-Tau / Aβ42	0.017 (0.010)	0.010 (0.002)	0.023 (0.012) $t = 4.584$ $P < 0.001^{***}$	0.027 (0.011) $t = 6.460$ $P < 0.001^{***}$	0.035 (0.009) $t = 12.051$ $P < 0.001^{***}$
FCSRT Total recall	44.292 (3.989)	43 (5.053)	45.091 (3.054) $t = 1.616$ $P = 0.117$	45 (2.619) $t = 1.384$ $P = 0.192$	45 (2.082) $t = 1.004$ $P = 0.348$
FCSRT Retention Index	0.980 (0.066)	0.980 (0.077)	0.981 (0.055) $t = 0.036$ $P = 0.959$	0.976 (0.058) $t = -0.171$ $P = 0.871$	0.973 (0.033) $t = -0.219$ $P = 0.833$
FCSRT Delayed cued recall	3.708 (1.675)	3.667 (1.910)	3.454 (1.683) $t = -0.373$ $P = 0.725$	3.867 (1.552) $t = 0.325$ $P = 0.768$	3.429 (1.902) $t = -0.280$ $P = 0.818$
FCSRT Delayed free recall	11.479 (1.935)	11.222 (2.315)	12 (1.746) $t = 1.211$ $P = 0.246$	11.467 (1.652) $t = 0.343$ $P = 0.796$	12 (2) $t = 0.780$ $P = 0.491$
FCSRT Total free recall	28.562 (5.379)	27.889 (6.173)	29.545 (5.466) $t = 0.900$ $P = -0.388$	28.267 (4.448) $t = 0.198$ $P = 0.851$	26.857 (5.014) $t = -0.393$ $P = 0.709$
FCSRT Total cued recall	15.729 (4.409)	15.111 (4.071)	15.545 (4.426) $t = 0.320$ $P = 0.767$	16.733 (4.061) $t = 1.141$ $P = 0.270$	18.143 (4.413) $t = 1.635$ $P = 0.122$
FCSRT Total delayed recall	15.187 (1.214	14.889 (1.323)	15.454 (0.800) $t = 1.669$ $P = 0.109$	15.333 (0.816) $t = -0.298$ $P = -1.132$	15.429 (0.534) $t = 1.035$ $P = 0.378$
WAIS IV Visual Puzzles Total Score	13.083 (4.297	13.222 (4.023)	12.818 (4.837) $t = -0.283$ $P = 0.804$	12.867 (4.103) $t = -0.250$ $P = 0.830$	12.143 (4.670) $t = -0.577$ $P = 0.604$
CRQ score	16.479 (3.724)	15.778 (4.427)	16.454 (3.188) $t = 0.561$ $P = 0.587$	16.867 (3.623) $t = 0.763$ $P = 0.471$	15.429 (3.690) $t = -0.185$ $P = 0.878$
Years of education	13.750 (3.778)	13.444 (3.959)	13.727 (3.588) $t = 0.237$ $P = 0.832$	13.800 (3.950) $t = 0.830$ $P = 0.257$	13.000 (3.697) $t = -0.256$ $P = 0.819$
Hippocampal volume / TIV	0.005 (0.001)	0.005 (0.001)	0.005 (0.001) $t = 0.444$ $P = 0.665$	0.005 (0.001) $t = 0.555$ $P = 0.587$	0.005 (0.001) $t = -0.1865$ $P = 0.854$
Hippocampal downregulation NF score	−0.038 (0.462)	−0.098 (0.437)	−0.049 (0.473) $t = 0.334$ $P = 0.743$	0.0475 (0.524) $t = 0.871$ $P = 0.386$	−0.043 (0.568) $t = 0.259$ $P = 0.796$
Mean EC in CA1	0.282 (0.040)	0.290 (0.037)	0.272 (0.043) $t = -1.383$ $P = 0.178$	0.283 (0.043) $t = -0.497$ $P = 0.622$	0.277 (0.054) $t = -0.717$ $P = 0.486$

Aβ42 = amyloid-β_{42}; CRQ = Cognitive Reserve Questionnaire; F = Female; FSCRT = Free and Cued Selective Reminding Test; M = male; NF = neurofeedback; PreAD = preclinical Alzheimer's disease; t = average t-statistic from 10 000 non-parametric permutation tests, comparing each category to controls; TIV = total intracranial volume. Asterisks denote uncorrected significance at conventional alpha levels.

was validated in a larger partly independent sample (77% overlap), by showing that hippocampal downregulation was associated with genetic predisposition to Alzheimer's disease, neurodevelopmental processes and bilateral cohesion of hippocampal function (Skouras et al., 2019b).

The VR environment had been developed in the game-engine Unity (Unity Technologies ApS, San Francisco, USA) (Fig. 1). During a 30-min long scanning session, participants were immersed in the VR environment and could run in a fixed, circular path. The experimental task was to explore different mental strategies, aiming to achieve the maximum velocity and to traverse the maximum distance possible, while at the same time attending to features of the VR environment, remembering them and considering whether they changed between each lap of the environment. Debriefing interviews revealed that most participants tried similar simple strategies, such as internal self-motivational speech, imagining that they were on a speeding vehicle, or focusing their sight on a specific point in the field of view. The first 30 functional volumes of the session served to establish a baseline of hippocampal activity, for each participant. Subsequently, with every repetition time, the most recent shift in hippocampal CA1 activity was compared to reference measures of change derived from the preceding 90 s (30 functional volumes; see 'Online functional image processing and neurofeedback' section). A 5% decrease of VR velocity was triggered by increases in hippocampal activity and a 5% increase of velocity was triggered by decreases in hippocampal activity. At any given moment, the current velocity was displayed as a percentage of the maximum velocity possible and a green or red signal was superimposed on a coronal brain view, reflecting the direction of the most recent change (Fig. 1). Every 30 volumes, the velocity was reset to 50%, resulting in 19 trials per session. The trials were not related to the experimental design from a statistical perspective, because computing EC requires hundreds of continuous functional volumes; however, having distinct trials served three important purposes. First, by resetting the speed every 90 s, all participants had a similar gamified experience, regardless of their actual performance. This was important from an ethical perspective because participants were aware that the gamified task, even though experimental, could be reflecting aspects of their brain function and health. It was therefore important that all participants would exit from the scanning session with an overall positive experience (and without any reason to worry) and this was also a secondary motivation to implement an online analysis pipeline with adaptive difficulty, based on a sliding-window baseline (see 'Online functional image processing and neurofeedback' section). Second, by resetting the speed and adapting the difficulty of the task, all participants had a similar overall sensory and perceptual experience. This was important to control for the effects of potential confounding factors such as individual differences in visual cortex activity during the scanning sessions. Third, resetting the speed enabled the developed paradigm to utilize effectively the basic principles of operant conditioning and sensory-aided learning. Because in the context of the gamified goal accelerations are perceived to be of positive valence and decelerations are perceived to be of negative valence, the 570 neurofeedback signals that occurred during each 30-min scanning session acted as positive and negative reinforcers, respectively. Thus, resetting the speed at regular intervals was necessary to avoid ceiling or floor effects that could compromise the number of reinforcers produced in a particular session.

Online functional image processing and neurofeedback

In each rt-fMRI session, EPI (echo planar imaging) images of whole-brain activity were acquired, reconstructed and exported every 3 s. The first 10 functional volumes were discarded to allow for gradient and tissue excitation levels to stabilize (Soares et al., 2016). Online movement correction through rigid-body registration was performed relative to an initial reference volume. To remove low frequency drifts in the functional MRI time series, temporal high-pass filltering with a cut-off frequency of 1/200 Hz (Tarvainen et al., 2002) was applied in real-time. An initial baseline mean and standard deviation were computed based on the first 30 processed functional volumes, during which the VR movement velocity remained constant at 0.5. Subsequently, voxel-efficiency weighting (Stoeckel et al., 2014) was performed by normalizing new images based on the mean and standard deviation of the preceding 30 observations in each voxel, according to Equation 1:

$$z_t = \frac{X_t - \overline{X}_{(t-30-1).(t-1)}}{\sigma_{(t-30-1).(t-1)}} \qquad (1)$$

where, at time t, X_t represents the filtered value of a single voxel, $\overline{X}_{(t-30-1).(t-1)}$ represents the mean of that voxel's time series within a time-window of 30 volumes up to time $(t-1)$, $\sigma_{(t-30-1).(t-1)}$ represents the corresponding standard deviation and z_t represents the efficiency-weighted value of the voxel. The length of the sliding window was set to 30 as a trade-off between the speed of adaptation and the reliability of the mean estimates, in accordance with generic statistical guidelines and the central limit theorem (Hogg et al., 1977). For each acquired functional volume, an outcome variable was instantiated for the activity measured within each participant's hippocampal CA1 region of interest, in native space, based on the following computations. At any given time point t_0, a voxel-wise expected data vector Y was computed according to Equation 2.

$$\mathbf{Y}(t_0) = \sum_{t=(t_0-30-1)}^{t_0-1} \frac{\mathbf{Z}(t)}{30} \qquad (2)$$

where $Z(t)$ represents the voxel-wise observed data vector composed of the output of Equation 1 for all voxels within the region of interest at time t. A non-linear metric neurofeedback metric (NF) was computed for each new volume, in real-time, according to Equation 3.

$$\mathbf{NF} = \overline{\mathbf{Z}}(t_0) - \overline{\mathbf{Y}}(t_0) \qquad (3)$$

With every repetition time, if the average expected signal surpassed the average observed signal in the hippocampal CA1 region of interest, the velocity v in the VR environment increased by 5% according to Equation 4; in the opposite case, the velocity decreased by 5% according to Equation 5, where v represents the VR movement velocity in the range {0.1, 1}.

$$NF < 0 \rightarrow \Delta v = 0.05 \qquad (4)$$

Table 2 Assessment of non-collinearity between measured variables

	Age	Amyloid-β_{42}	p-tau	T-tau	p-tau/amyloid-β_{42}
Age	–	R = 0.129 P = 0.382	R = 0.369 P = 0.010**	R = 0.373 P = 0.009**	R = 0.224 P = 0.126
Amyloid-β_{42}	R = 0.129 P = 0.382	–	R = 0.195 P = 0.184	R = 0.276 P = 0.057	R = –0.580 P < 0.001***
P-tau	R = 0.369 P = 0.010*	R = 0.195 P = 0.184	–	R = 0.987 P < 0.001***	R = 0.625 P < 0.001***
T-tau	R = 0.373 P = 0.009**	R = 0.276 P = 0.057	R = 0.987 P < 0.001***	–	R = 0.553 P < 0.001***
P-tau / amyloid-β_{42}	R = 0.224 P = 0.126	R = –0.580 P < 0.001***	R = 0.625 P < 0.001***	R = 0.553 P < 0.001***	–
APOE ε4 allele carrier status	R = –0.699 P < 0.001***	R = –0.325 P = 0.024*	R = –0.288 P = 0.047*	R = –0.290 P = 0.046*	R = 0.025 P = 0.864
FCSRT Total recall	R = –0.177 P = 0.227	R = –0.202 P = 0.168	R = 0.004 P = 0.976	R = 0.014 P = 0.921	R = 0.125 P = 0.398
FCSRT Retention Index	R = 0.088 P = 0.554	R = 0.065 P = 0.658	R = –0.046 P = 0.756	R = –0.015 P = 0.921	R = –0.083 P = 0.576
FCSRT Delayed cued recall	R = 0.250 P = 0.087	R = –0.026 P = 0.861	R = 0.143 P = 0.331	R = 0.107 P = 0.468	R = 0.156 P = 0.291
FCSRT Delayed free recall	R = –0.217 P = 0.138	R = –0.087 P = 0.558	R = –0.129 P = 0.383	R = –0.090 P = 0.543	R = –0.073 P = 0.621
FCSRT Total free recall	R = –0.307 P = 0.033	R = 0.016 P = 0.913	R = –0.128 P = 0.387	R = –0.089 P = 0.547	R = –0.137 P = 0.353
FCSRT Total cued recall	R = 0.239 P = 0.101	R = –0.219 P = 0.134	R = 0.175 P = 0.233	R = 0.133 P = 0.369	R = 0.305 P = 0.035*
FCSRT Total delayed recall	R = 0.004 P = 0.978	R = –0.197 P = 0.180	R = –0.005 P = 0.974	R = 0.008 P = 0.956	R = 0.114 P = 0.439
WAIS IV Visual Puzzles Total Score	R = –0.397 P = 0.005	R = 0.092 P = 0.535	R = –0.112 P = 0.447	R = –0.106 P = 0.475	R = –0.190 P = 0.196
CRQ score	R = –0.012 P = 0.935	R = 0.046 P = 0.755	R = 0.013 P = 0.927	R = 0.025 P = 0.868	R = –0.081 P = 0.582
Years of education	R = –0.208 P = 0.156	R = –0.018 P = 0.901	R = –0.137 P = 0.354	R = –0.118 P = 0.424	R = –0.091 P = 0.540
Hippocampal volume / TIV	R = –0.026 P = 0.859	R = –0.012 P = 0.933	R = 0.044 P = 0.764	R = 0.068 P = 0.645	R = –0.025 P = 0.864
Hippocampal downregulation NF score	R = 0.219 P = 0.135	R = 0.087 R = 0.557	R = 0.215 P = 0.143	R = 0.198 P = 0.176	R = 0.115 P = 0.434
Mean EC in CA1	R = 0.164 P = 0.264	R = 0.219 P = 0.135	R = –0.019 P = 0.898	R = 0.017 P = 0.908	R = –0.172 P = 0.242

CRQ = Cognitive Reserve Questionnaire; FSCRT = Free and Cued Selective Reminding Test; NF = neurofeedback; TIV = total intracranial volume.
Asterisks denote uncorrected significance at conventional alpha levels.

$$NF > 0 \rightarrow \Delta v = -0.05 \qquad (5)$$

Offline functional image processing

Raw images were processed and examined using a well-controlled combination of highly specialized functions from open-source neuroimaging software. To maximize cortical segmentation accuracy, T_1 images were subjected to the N4 non-parametric non-uniform intensity normalization bias correction function (Tustison *et al.*, 2010, 2013) of the Advanced Normalization Tools (ANTs; version 2.x, committed in January 2016; Avants *et al.*, 2009) and to an optimized blockwise non-local means denoising filter (Coupé *et al.*, 2008). SPM12 (Statistical Parametric Mapping, RRID: SCR_007037) together with VBM8 (VBM toolbox, RRID: SCR_014196), were used to segment each anatomical image into grey matter, white matter and CSF. Whole-brain images with removed cranium were also derived and used for normalization. Neuroanatomically-plausible symmetric diffeomorphic matrices were computed to transform each subject's anatomical data to a custom template derived from the same population (Skouras *et al.*, 2019a) and subsequently to MNI space (Avants *et al.*, 2011; Tustison and Avants, 2013) as defined by the robust, high-definition ICBM (International Consortium for Brain Mapping) brain template (Fonov *et al.*, 2011), also with removed cranium. All transformation matrices were concatenated and applied to the CA1 region of interest masks and functional MRI datasets in a single step to ensure optimal normalization while avoiding multiple interpolations, in accordance with best image processing practices.

Using SPM12 and the MIT connectivity toolbox (Connectivity Toolbox, RRID: SCR_009550), functional data were subjected to standard preprocessing, consisting of
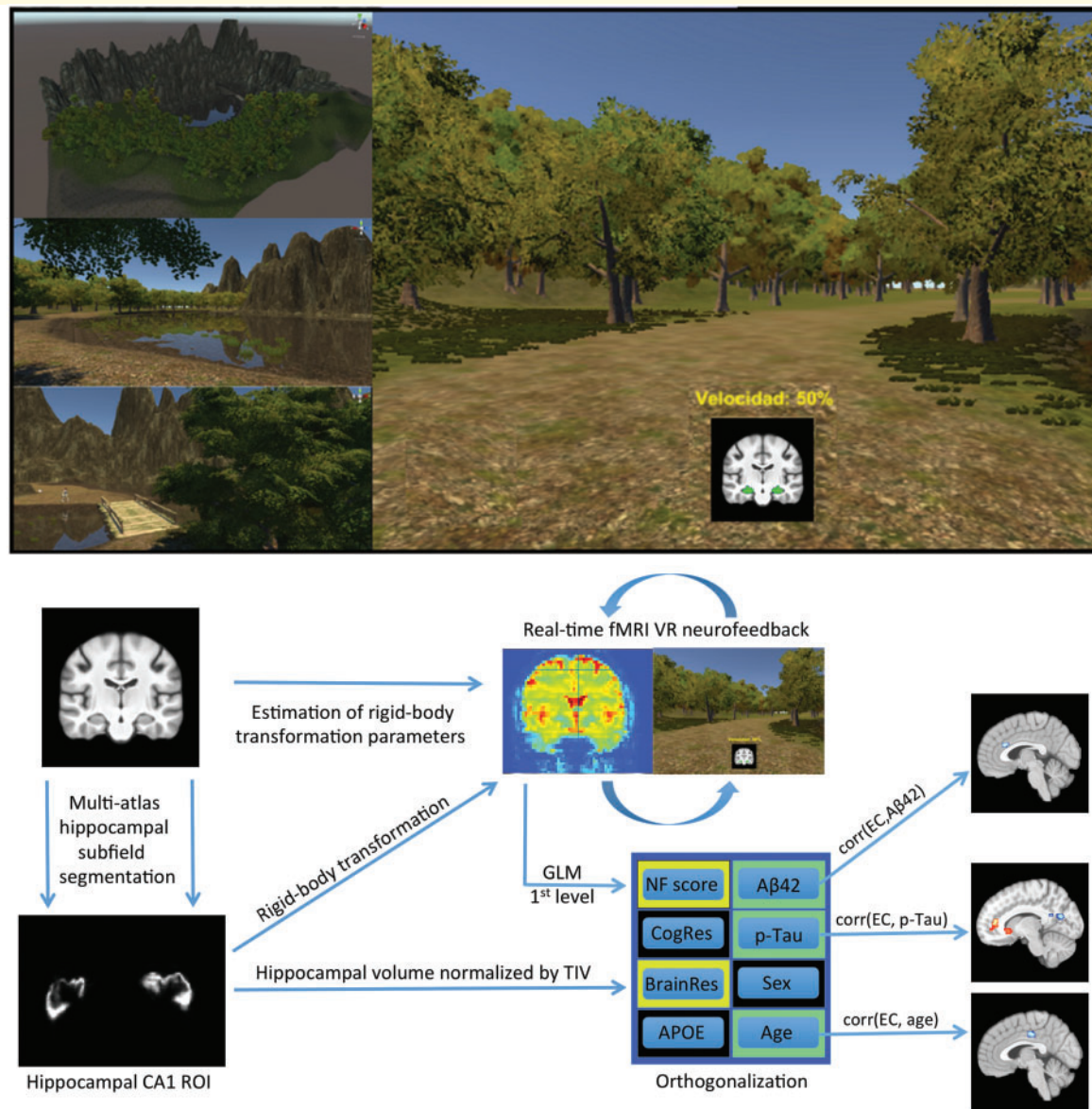
Figure 1 VR environment and neuroimaging pipeline. The VR neurofeedback paradigm developed for the study used principles of passive, sensory-aided, operant conditioning and featured 570 neurofeedback signals per session. To maintain a balanced perceptual experience across participants, task difficulty adapted to individual performance dynamically, aiming to drive CA1 activity in each participant to the minimum possible. Using previously acquired anatomical images, multi-atlas hippocampal subfield segmentation localized and segmented hippocampal subfield CA1, prior to real-time scanning. With every real-time functional volume, moment-to-moment changes in hippocampal CA1 activation effected inverse changes of velocity in VR. Offline statistical modelling was used to derive a measure of neurofeedback regulation performance and to perform EC mapping (i.e. to estimate how much influence each voxel exerts during hippocampal CA1 downregulation with neurofeedback). *APOE* = apolipoprotein genotype; $A\beta42$ = amyloid-β_{42}; BrainRes = brain reserve; CA1 = cornu ammonis 1; CogRes = cognitive reserve; fMRI = functional MRI; GLM = general linear model; NF = neurofeedback; p-tau = phosphorylated tau; ROI = region of interest; TIV = total intracranial volume.

slice-time correction, realignment and reslicing of functional volumes, denoising via regression of average white matter timeseries, average CSF timeseries, 24 Volterra expansion movement parameters and scan-nulling regressors (Lemieux *et al.*, 2007) produced by the Artifact Detection Tools (ART; RRID: SCR_005994). Each subject's functional data were masked by the grey matter of their equivalent anatomical datasets using FSL and then normalized to MNI space in accordance with their respective diffeomorphic matrices using ANTs. Temporal high-pass filtering with a cut-off frequency of 1/90 Hz and spatial smoothing using a 3D Gaussian kernel and a filter size of 6 mm full-width at half-maximum, were performed using the Leipzig Image Processing and Statistical Inference Algorithms (LIPSIA v2.2.7, 2011, RRID: SCR_009595; Lohmann *et al.*, 2000).

EC was computed for every voxel, based on the LIPSIA implementation of ECM (vecm command), with previously published detailed mathematical specification (Lohmann *et al.*, 2010). In effect, the ECM procedure begins by computing a correlation coefficient between every possible pair of voxels within the computational volume (e.g. grey matter mask), based on their time series. It then assigns to each voxel an initial centrality value that is computed as the sum of all correlation coefficients that exist between that voxel and all other voxels (a value equivalent to degree centrality). Subsequently, ECM updates the centrality value in each voxel iteratively, each time by a weighted sum of its correlation coefficients with other voxels, using weights that correspond to each paired voxel's centrality value from the previous iteration. The iterations repeat until the values stabilize and there is no further change from one iteration to the next. Importantly, we limited the similarity matrix to positive correlations between grey matter voxels, similarly to our previous Alzheimer's disease study with EC (Skouras *et al.*, 2019*a*). EC values were Gaussianized voxel-wise across all subjects to enable second-level parametric inference, using a general transformation designed to optimize the reliability of arbitrary distributions (Albada and Robinson, 2007). The resulting whole-brain images entered second level statistical modelling and voxel-wise multiple regression analyses (see 'Statistical analysis' section).

Statistical analysis

For standard type I and II error rates (α = 0.05, β = 0.20), *a priori* computations of required sample size were performed using statistical power estimation software (G*Power v 3.1; RRID: SCR_013726; Faul *et al.*, 2007, 2009). The computations suggested that to enable sufficient statistical power for effects of medium size ($f^2 > 0.15$), using multiple regression with up to seven predictor variables, a minimum sample size of 43 subjects would be required. Pearson's r was used as a metric of similarity in first-level general linear model (GLM) to quantify neurofeedback performance per participant. A linear vector coding continuous downregulation, as the target performance for neurofeedback, was compared to neurofeedback moment-to-moment regulation, measured by the re-aligned average CA1 time series, to produce a measure of neurofeedback performance for each participant similar to a previous study (Skouras and Scharnowski, 2019). First, we investigated whether the unique variance associated with CSF amyloid-β_{42} levels was reflected in EC during the neurofeedback task. For consistency, CSF amyloid-β_{42} values were multiplied by –1 during modelling, to align results and colour maps with the direction of the pathophysiological continuum of Alzheimer's disease. CSF amyloid-β_{42} values were orthogonalized to potential confounding variables; specifically sex, age, number of *APOE* ε4 alleles, hippocampal volume, cognitive reserve and neurofeedback performance. This resulted in an orthogonal second-level design matrix that was used for GLM of the unique effect of amyloid-β_{42} on EC during VR neurofeedback. The resulting whole-brain z-map was corrected for multiple comparisons using 10 000 iterations of Monte Carlo simulations, with a pre-threshold of $z > 2.326$ ($P < 0.01$) and a corrected significance level of $P < 0.05$. Similarly, we investigated for a possible correlation between p-tau and EC, controlling for the same confounding variables.

Finally, we investigated the effect of healthy ageing on EC during VR neurofeedback, by orthogonalizing age to all potential confounding factors, including the CSF p-tau by amyloid-β_{42} ratio (Maddalena *et al.*, 2003). All second-level neuroimaging analyses featured data from the entire sample. All scale variables were normalized prior to orthogonalization via the recursive Gram-Schmidt orthogonalization of SPM12 (SPM, RRID: SCR_007037). For quality control, we confirmed that each variable of interest was completely orthogonal to all covariates in its respective design matrix, as well as to all original vector data, while remaining in high correlation with its own original vector. This ensured investigating meaningful observations and effects due to the unique variance in each variable of interest.

Code and data availability

The VR environment and the analysis software developed for the experiment, are publicly available as open-source software via the 'VR_multipurpose_v1.0' and the 'HippDownReg_exp1' repositories (GitHub; RRID: SCR_002630), respectively. Data used can been made available to researchers for non-commercial purposes, following agreement and approval by the Barcelonaβeta Brain Research Center's Data and Publications Committee.

Results

Amyloid-β_{42}

Controlling for the effects of age, sex, number of *APOE* ε4 alleles, hippocampal volume, cognitive reserve and neurofeedback performance, CSF amyloid-β_{42} levels showed a significant positive correlation with EC in the ACC [Brodmann area (BA)24, BA32] and primary motor cortex (BA4) (Fig. 2 and Table 3). Note that amyloid-β_{42} levels in CSF are inversely proportional to the extent of amyloid-β plaque accumulation in the brain (Strozyk *et al.*, 2003; Grothe *et al.*, 2017); i.e. abnormal amyloid-β_{42} biomarkers were related to low EC in the ACC and BA4.

Phosphorylated-tau

Controlling for the effects of age, sex, number of *APOE* ε4 alleles, hippocampal volume, cognitive reserve and neurofeedback performance, p-tau levels in CSF showed a significant positive correlation with EC in the ACC (BA32, BA10) ventral striatum (caudate, nucleus accumbens, putamen) and left primary somatosensory cortex (BA2). CSF p-tau levels, also showed a significant negative correlation with EC in the posterior cingulate cortex, precuneus, cuneus and left frontal pole (BA9) (Fig. 3 and Table 3).

Healthy ageing

Controlling for the effects of sex, number of *APOE* ε4 alleles, hippocampal volume, cognitive reserve,

neurofeedback performance and the CSF p-tau by amyloid-β_{42} ratio (Maddalena *et al.*, 2003), age presented a significant negative correlation with EC in the midcingulate cortex, insula, primary somatosensory cortex (BA2) and inferior parietal lobule (BA40). Age also presented a significant positive correlation with EC in the inferior temporal gyri (Fig. 4 and Table 3).

Discussion

Adding to our knowledge, this is the first real-time neurofeedback study using CSF biomarker data. The results in cognitively unimpaired participants at risk for Alzheimer's disease corroborate that differences of EC in the cingulate cortex play an important role in the pathophysiological continuum of Alzheimer's disease and show for the first time that such differences may begin at a very early pathophysiological stage. The latter finding suggests that hippocampal self-regulation tasks, enabling functional connectomic analyses, can be of benefit in revealing information of clinical relevance to Alzheimer's disease progression.

During hippocampal downregulation, the decreased EC in the ACC and primary motor cortex, which is associated with abnormally decreased CSF amyloid-β_{42} levels and, by extension, to increased amyloid-β plaque deposition in the brain, stands out as a potential neural correlate of elevated amyloid deposition, particularly because the ACC is among the first regions where amyloid deposition can be detected with PET imaging (Grothe *et al.*, 2017). Because of the characteristics of our sample (Tables 1 and 2), these findings represent early pathophysiological alterations, without objectively measurable impact on overall memory performance, that relate to the brain network involved in the regulation of hippocampal hyperactivity. They suggest that in subjects with abnormal amyloid-β_{42} deposition, the ACC is less influential in regulating hippocampal CA1 (adjusted for risk factors and task performance). According to current models, the ACC, together with the anterior insula, as well as parts of the prefrontal cortex, parietal lobule, ventral striatum and thalamus, comprise the brain network that is primarily responsible for learning to voluntarily regulate other brain areas through neurofeedback training (Sitaram *et al.*, 2017). The perspective provide a mechanistic explanation for the reason most of these areas, specifically, are engaged by the present VR neurofeedback paradigm, leading to enhanced sensitivity in relation to early alterations of their connectivity and systemic network function.

With elevated CSF p-tau levels, EC decreases in the prefrontal cortex and the posterior cingulate cortex, while EC increases in the ACC and ventral striatum; i.e. during early stages, amyloid-β_{42} accumulation in the brain and tau
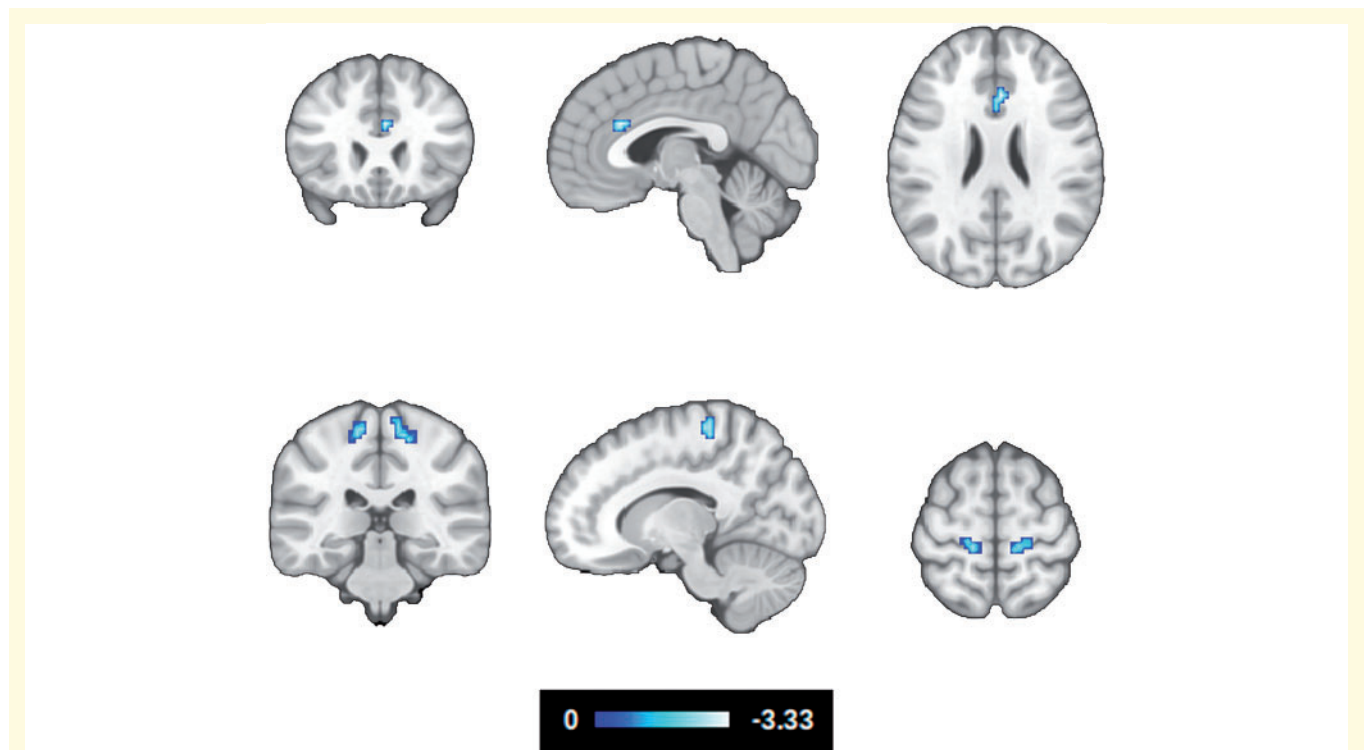

Figure 2 Correlation between eigenvector centrality during hippocampal downregulation and amyloid-β deposition. The effects of age, sex, number of *APOE* ε4 alleles, hippocampal volume, cognitive reserve and neurofeedback performance, were modelled and controlled ($z > 2.326$, $P < 0.05$ whole-brain corrected, 95% confidence interval). Note that CSF amyloid-β_{42} levels are inversely proportional to the extent of amyloid-β plaque deposition in the brain.

Table 3 Results of ECM in relation to CSF biomarkers and age, corrected for whole-brain multiple comparisons ($P < 0.05$)

Brain regions	MNI coordinates, x y z	Cluster size, mm³	z-value, max (mean)
Amyloid-β correlation with EC during CA1 downregulation			
ACC, BA24, BA32	3 24 28	405	−3.34 (−2.65)
L BA4	−21 −27 70	405	−2.73 (−2.49)
R BA4	18 −33 61	594	−2.91 (−2.56)
P-tau correlation with EC during CA1 downregulation			
ACC, BA32 (BA10)	12 42 13	513	3.31 (2.66)
R Caudate, NAc, Putamen	15 21 −2	513	3.53 (2.86)
L Caudate, NAc, Putamen	−12 18 −5	756	3.84 (2.87)
L BA2	−57 −24 43	297	3.54 (2.79)
PCC, PCu, R Cu	21 −66 22	1674	−3.36 (−2.69)
L Frontal pole, BA9	−27 51 43	297	−4.00 (−2.68)
Age correlation with EC during CA1 downregulation			
R ITG	57 −54 −23	1539	4.62 (3.01)
R ITG	57 −21 −32	837	3.94 (2.83)
L ITG	−63 −45 −20	999	3.38 (2.77)
L ITG	−57 −18 −29	459	2.98 (2.65)
MCC, BA24, BA31	−6 −21 43	1593	−4.10 (−2.94)
R BA40, BA2	57 −24 37	2565	−4.26 (−2.83)
L BA40, BA2	−54 −30 28	675	−3.92 (−2.89)
R Insula, BA13	42 6 −5	297	−3.15 (−2.75)
L Insula, BA13	−36 3 −2	648	−3.35 (−2.60)

The fourth column indicates the maximal z-value of voxels within a cluster (with the mean z-value of all voxels within a cluster in parentheses). CSF amyloid-β_{42} and p-tau levels were orthogonalized to age, sex, number of *APOE* ε4 alleles, cognitive reserve, brain reserve and hippocampal downregulation performance. For consistency, CSF amyloid-β_{42} values were multiplied by −1 during modelling, to align results and colour maps with the direction of the pathophysiological continuum of Alzheimer's disease. Age was orthogonalized to the CSF p-tau by amyloid-β_{42} ratio, sex, number of *APOE* ε4 alleles, cognitive reserve, brain reserve and hippocampal downregulation performance. BA = Brodmann area; Cu = cuneus; L = left; MCC = midcingulate cortex; MNI = Montreal Neurological Institute; NAc = nucleus accumbens; PCC = posterior cingulate cortex; PCu = precuneus; p-tau = phosphorylated tau; R = right.

phosphorylation seem to have opposite effects on EC in the ACC. The ACC is also involved in the brain signature of cognitive resilience, which is related to its metabolic capacity (Arenaza-Urquijo *et al.*, 2019). The possibility of EC in the ACC initially decreasing and later on increasing, in early response to the subsequent steps of a pathophysiological cascade, resembles the concurrent pattern of default mode network (DMN) connectivity, which increases proportionally to CSF amyloid-β_{42} levels within the range of normal amyloid values, but decreases proportionally to CSF amyloid-β_{42} levels within the elevated range of abnormal amyloid accumulation (Palmqvist *et al.*, 2017). This is supported by the decrease of EC in the posterior cingulate cortex/precuneus/cuneus that comprises the main DMN hub (Smith *et al.*, 2009; Andrews-Hanna *et al.*, 2010; Spreng and Grady, 2010). Moreover, recent evidence suggests that baseline EC in the posterior cingulate cortex/precuneus region is predictive of first-session DMN neurofeedback regulation learning (Skouras and Scharnowski, 2019). Overall, the EC differences associated with increased CSF p-tau levels and by extension to the formation of neurofibrillary tangles in the brain, resemble results found in advanced patients with Alzheimer's disease with dementia, in the ACC and occipital cortex (Binnewijzend *et al.*, 2014). In this context, the present results corroborate the most relevant literature and support

shifting the timeframe for the detection of aberrant functional alterations, earlier than previously evidenced, to the presymptomatic stage of Alzheimer's disease. Of particular importance, the present findings suggest that aberrant EC initially precedes neurodegeneration, rather than resulting from it. This is supported by complementary evidence showing minimal overlap between the ACC cluster and regions with grey matter reductions in patients with Alzheimer's disease (Binnewijzend *et al.*, 2014).

Left BA8, the cluster presenting decreased EC in the left prefrontal cortex, is one of the main loci of autobiographical memory (Janata, 2009) and appears to be suitable as an accessible target region for non-invasive neurostimulation intervention studies (Reinhart and Nguyen, 2019). Following the interpretational framework proposed by recent work with resting-state EC and Alzheimer's disease CSF biomarkers (Skouras *et al.*, 2019*a*), given the involvement of the ACC, PFC and ventral striatum in the neurofeedback learning network (Sitaram *et al.*, 2017), it is feasible that the decreasing EC of the PFC is being compensated by increasing EC in the ACC and ventral striatum; the latter of which is affected by amyloid deposition only at a relatively advanced stage (Grothe *et al.*, 2017). Considering the crucial roles of the hippocampus, ventral striatum and cingulate in affective processing (Dalgleish, 2004), these findings support proposing that
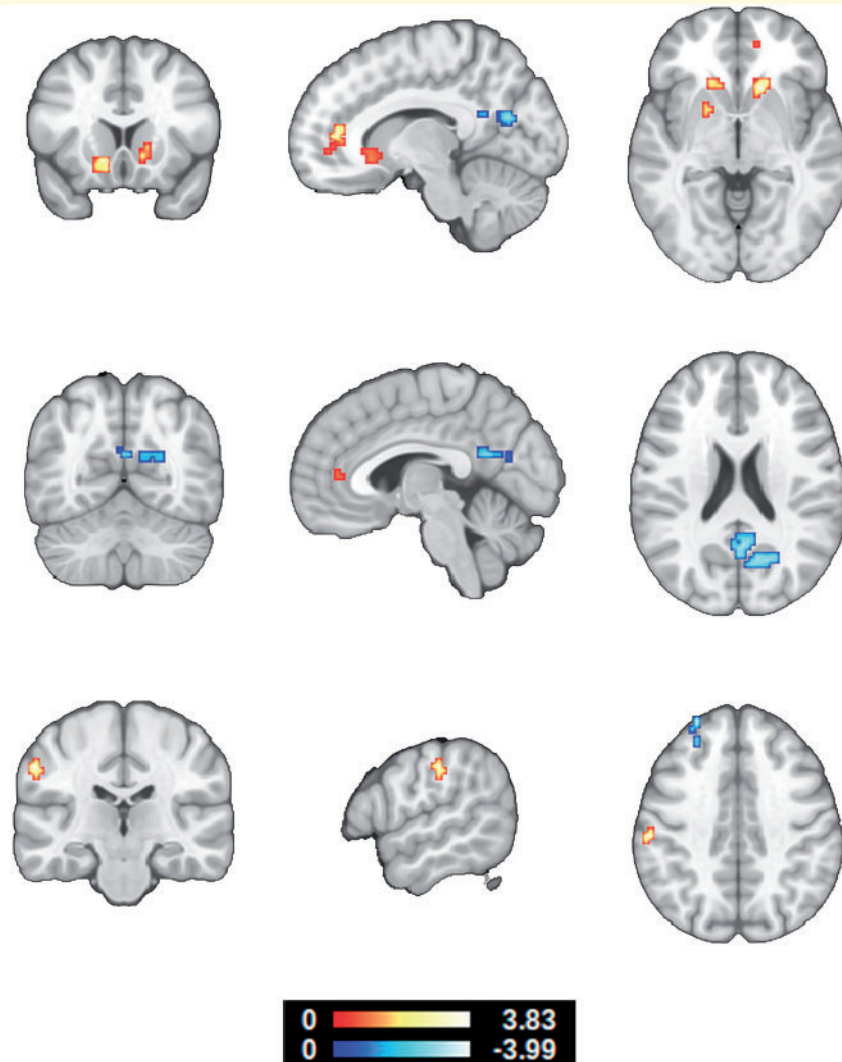
Figure 3 Correlation between eigenvector centrality during hippocampal downregulation and CSF p-tau levels. The effects of age, sex, number of *APOE* ε4 alleles, hippocampal volume, cognitive reserve and neurofeedback performance were modelled and controlled ($z > 2.326$, $P < 0.05$ whole-brain corrected, 95% confidence interval). Note that CSF p-tau levels are proportional to the presence of neurofibrillary tangles in the brain. These results suggest that Alzheimer's disease-characteristic EC differences in the ACC may occur earlier than previously believed.

some of the earliest effects along the pathophysiological continuum of Alzheimer's disease are related to dysfunctions of affective processing, similar to almost all neuropsychiatric pathologies (Connan *et al.*, 2003; Leppänen, 2006; Hoekert *et al.*, 2007; Mannie *et al.*, 2007; Kang *et al.*, 2012). Additionally, in a mouse model of Alzheimer's disease, selective neurodegeneration in the ventral tegmental area (VTA) at pre-plaque stages, resulted in lower dopamine outflow in the hippocampus and nucleus accumbens and correlated with impairments of synaptic plasticity in CA1, as well as memory deficits and dysfunction of reward processing (Nobili *et al.*, 2017). The VTA is particularly responsive to neurofeedback training (Macinnes *et al.*, 2016) and outgoing fibres from the VTA connect directly to the hippocampus (Gasbarri

et al., 1994; Penner and Mizumori, 2012). Thereby, it is also feasible that the increased EC in the dopaminergic ventral striatum compensates for early aberrancies in VTA function that are undetectable with 3 T whole-brain functional MRI. In addition, a contemporary model proposes that the hippocampus, the prefrontal cortex and the VTA, form the most crucial components of the long-term memory network (Penner and Mizumori, 2012).

As hypothesized, during hippocampal downregulation, cognitively unimpaired subjects with elevated CSF p-tau levels, exhibit a similar increase in EC, as the one present during resting state in patients with Alzheimer's disease (Binnewijzend *et al.*, 2014), despite important improvements in normalization methods across studies (Avants *et al.*, 2008; Klein *et al.*, 2009). This corroborates a
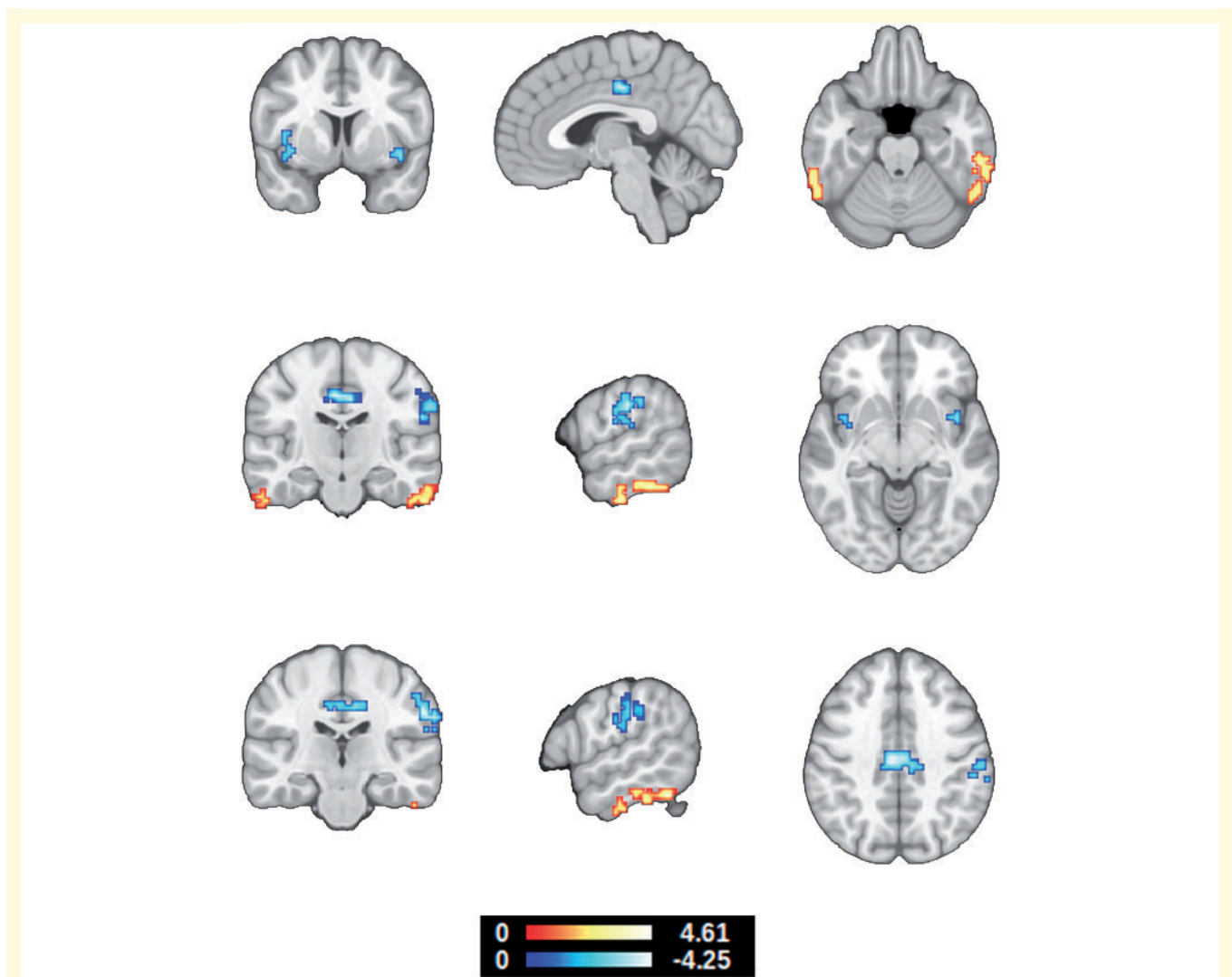
Figure 4 Correlation between eigenvector centrality during hippocampal downregulation and age. The effects of sex, number of *APOE* ε4 alleles, hippocampal volume, cognitive reserve, neurofeedback performance, CSF amyloid-β_{42} and p-tau levels were modelled and controlled ($z > 2.326$, $P < 0.05$ whole-brain corrected, 95% confidence interval). In relation to Fig. 3, these results show that EC in the cingulate and BA2 present the opposite patterns in healthy ageing.

replicable resting-state finding that was previously only measurable when investigating across control subjects and patients with dementia due to Alzheimer's disease (Binnewijzend *et al.*, 2014; Skouras *et al.*, 2019*a*). This observation suggests that the developed VR neurofeedback task may indeed be hypersensitive to preclinical alterations in brain function. In contrast, an important effect of healthy ageing is decreased EC in the cingulate cortex, during hippocampal downregulation. This corroborates previous evidence from task-free functional MRI, showing that healthy older adults (mean age = 63, SD = 7) present significantly lower EC in the cingulate than healthy younger adults (mean age = 24, SD = 4; Antonenko *et al.*, 2018). Overall, the effect of healthy ageing on EC across the cingulate cortex (Fig. 4) is opposite to that of elevated CSF p-tau levels (Fig. 3), clinical

symptoms (Binnewijzend *et al.*, 2014), and Alzheimer's disease progression (Skouras *et al.*, 2019*a*). Thereby, current evidence suggests that the cingulate decreases in centrality in healthy ageing and increases in centrality in Alzheimer's disease, with noticeable differences even in a very early phase. The effect of healthy ageing on EC in the inferior temporal gyrus, points to the possibility that in healthy ageing, increasing resources are being devoted to semantic memory (Binney *et al.*, 2010). To our knowledge, there is no previous evidence of EC correlation with age in the inferior temporal gyrus; however, no previous ECM ageing study controlled for the effect of any CSF biomarkers. Moreover, recent evidence suggests cognitive decline may emerge from functional decoupling within a neural circuit composed of temporal and frontal regions, which is integral to monitoring real-world

information and storing it into memory (Reinhart and Nguyen, 2019).

In general, the EC findings could be different using a hippocampal upregulation task, because upregulation and downregulation learning can be negatively correlated (Skouras and Scharnowski, 2019). It is important to determine the specificity of the present findings to hippocampal downregulation tasks and to replicate them in longitudinal studies that include both downregulation and upregulation, as well as sham neurofeedback conditions. It is equally important to validate the tentative interpretations offered here, using the same self-regulation paradigm in studies involving patients with mild cognitive impairment. With these aims, we have made the developed VR environment publicly available as open-source software, to enable replication studies and multicentre investigations within a standard framework (see 'Code and data availability' section). The latter might enable the aggregation of sufficient datasets to derive accurate functional neuroimaging-based diagnostic models using machine learning algorithms.

As noted, four participants had a subjective impression of cognitive or memory decline, while their cognition was preserved based on objective cognitive testing. These participants did not present a consistently distinctive profile with regards to cognitive scores, hippocampal volume, genetics or CSF biomarkers. One participant was an *APOE* ε4 heterozygote with normal biomarkers, one was an *APOE* ε4 non-carrier with abnormal amyloid-β_{42} level but normal p-tau level, one was an *APOE* ε4 non-carrier with normal amyloid-β_{42} level but abnormal p-tau level, and one was an *APOE* ε4 heterozygote with abnormal amyloid-β_{42} level and abnormal p-tau level. However, all four participants were female, with a relatively high level of education or a relatively high hippocampal downregulation neurofeedback score. Descriptive statistics for these four participants, in relation to control and preclinical Alzheimer's disease participants are provided in Supplementary Table 2. Based on CSF data from a larger sample ($n = 261$) from the ALFA cohort, a subjective impression of cognitive or memory decline is relatively uninformative in the context of the present study. Therefore, we have considered the influence of the four described participants identically to that of the other participants, as ordinary instances within the biological and cognitive variability that exists in the healthy to preclinical range of the Alzheimer's disease continuum.

We have demonstrated that amyloid deposition results in aberrancy with regards to the functional brain network used to downregulate hippocampal subfield CA1. Further, significant differences in EC associated with CSF biomarkers in clinical Alzheimer's disease, are also measurable in presymptomatic stages. Moreover, we provide a standard paradigm to replicate and extend this work on a global level. This opens new avenues for further research applications, which quantify and monitor disease progression, by identifying early alterations in the self-regulation of brain function, with potential for non-invasive prognostic screening.

Competing interests

J.L.M. is a consultant for the following for-profit companies: Alergan, Roche diagnostics, Genentech, Novartis, Lundbeck, Oryzon, Biogen, Lilly, Janssen, Green Valley, MSD, Eisai, Alector, Raman Health. K.B. has served as a consultant or at advisory boards for Abcam, Axon, Biogen, Lilly, MagQu, Novartis and Roche Diagnostics, and is a co-founder of Brain Biomarker Solutions in Gothenburg AB, a GU Ventures-based platform company at the University of Gothenburg. H.Z. has served at scientific advisory boards for Roche Diagnostics, CogRx, Samumed and Wave, and has given lectures in symposia sponsored by Alzecure and Biogen, and is a co-founder of Brain Biomarker Solutions in Gothenburg AB, a GU Ventures-based platform company at the University of Gothenburg.

Supplementary material

Supplementary material is available at *Brain* online.

Appendix 1

Collaborators of the ALFA study are: Anna Brugulat-Serrat, Raffaele Cacciaglia, Marta Crous-Bou, Carme Deulofeu, Ruth Dominguez, Xavi Gotsens, Oriol Grau-Rivera, Laura Hernandez, Gema Huesa, Jordi Huguet,

María León, Paula Marne, Tania Menchón, Marta Milà-Alomà, Grégory Operto, Maria Pascual, Albina Polo, Sandra Pradas, Aleix Sala-Vila, Gemma Salvadó, Gonzalo Sánchez-Benavides, Sabrina Segundo, Anna Soteras, Marc Suárez-Calvet, Laia Tenas, Marc Vilanova and Natalia Vilor-Tejedor.

References

Adriaanse SM, Wink AM, Tijms BM, Ossenkoppele R, Verfaillie SCJ, Lammertsma AA, et al. The association of glucose metabolism and eigenvector centrality in Alzheimer's disease. Brain Connect 2016; 6: 1–8.

Albada VS, Robinson PA. Transformation of arbitrary distributions to the normal distribution with application to EEG test–retest reliability. J Neurosci Methods 2007; 161: 205–11.

Alnæs D, Sneve MH, Richard G, Skåtun KC, Kaufmann T, Nordvik JE, et al. Functional connectivity indicates differential roles for the intraparietal sulcus and the superior parietal lobule in multiple object tracking. Neuroimage 2015; 123: 129–37.

Andrews-Hanna JR, Reidler JS, Sepulcre J, Poulin R, Buckner RL. Functional-anatomic fractionation of the brain's default network. Neuron 2010; 65: 550–62.

Antonenko D, Nierhaus T, Meinzer M, Prehn K, Thielscher A, Ittermann B, et al. Age-dependent effects of brain stimulation on network centrality. Neuroimage 2018; 176: 71–82.

Arenaza-Urquijo EM, Przybelski SA, Lesnick TL, Graff-Radford J, Machulda MM, Knopman DS, et al. The metabolic brain signature of cognitive resilience in the 80+: beyond Alzheimer pathologies. Brain 2019; 142: 1134–47.

Avants BB, Epstein CL, Grossman M, Gee JC. Symmetric diffeomorphic image registration with cross-correlation: evaluating automated labeling of elderly and neurodegenerative brain. Med Image Anal 2008; 12: 26–41.

Avants BB, Tustison N, Song G. Advanced normalization tools (ANTS). Insight 2009; 2: 1–35.

Avants BB, Tustison NJ, Song G, Cook PA, Klein A, Gee JC. A reproducible evaluation of ANTs similarity metric performance in brain image registration. Neuroimage 2011; 54: 2033–44.

Barulli D, Stern Y. Efficiency, capacity, compensation, maintenance, plasticity: emerging concepts in cognitive reserve. Trends Cogn Sci 2013; 17: 502–9.

Binnewijzend M, Adriaanse S, Flier W, Teunissen C, Munck J, Stam C, et al. Brain network alterations in Alzheimer's disease measured by Eigenvector centrality in fMRI are related to cognition and CSF biomarkers. Hum Brain Mapp 2014; 35: 2383–93.

Binney RJ, Embleton KV, Jefferies E, Parker GJM, Lambon R, Matthew A. The ventral and inferolateral aspects of the anterior temporal lobe are crucial in semantic memory: evidence from a novel direct comparison of distortion-corrected fMRI, rTMS, and semantic dementia. Cereb Cortex 2010; 20: 2728–38.

Blesa R, Pujol M, Aguilar M, Santacruz P, Bertran-Serra I, Hernandez G, et al. Clinical validity of the 'mini-mental state' for Spanish speaking communities. Neuropsychologia 2001; 39: 1150–7.

Bonacich P. Technique for analyzing overlapping memberships. Sociol Methodol 1972; 4: 176–85.

Borgatti SP. Centrality and network flow. Soc Netw 2005; 27: 55–71.

Cavedo E, Galluzzi S, Pievani M, Boccardi M, Frisoni GB. Norms for imaging markers of brain reserve. J Alzheimers Dis 2012; 31: 623–33.

Chirico A, Cipresso P, Yaden DB, Biassoni F, Riva G, Gaggioli A. Effectiveness of immersive videos in inducing awe: an experimental study. Sci Rep 2017; 7: 1218.

Connan F, Campbell I, Katzman M, Lightman S, Treasure J. A neurodevelopmental model for anorexia nervosa. Physiol Behav 2003; 79: 13–24.

Coupé P, Yger P, Prima S, Hellier P, Kervrann C, Barillot C. An optimized blockwise nonlocal means denoising filter for 3-D magnetic resonance images. IEEE Trans Med Imaging 2008; 27: 425–41.

Dalgleish T. The emotional brain. Nat Rev Neurosci 2004; 5: 583.

Dimsdale-Zucker HR, Ritchey M, Ekstrom AD, Yonelinas AP, Ranganath C. CA1 and CA3 differentially support spontaneous retrieval of episodic contexts within human hippocampal subfields. Nat Commun 2018; 9: 294.

Duarte IC, Ferreira C, Marques J, Castelo-Branco M. Anterior/posterior competitive deactivation/activation dichotomy in the human hippocampus as revealed by a 3D navigation task. PLoS One 2014; 9: e86213.

Dubois B, Feldman HH, Jacova C, DeKosky ST, Barberger-Gateau P, Cummings J, et al. Research criteria for the diagnosis of Alzheimer's disease: revising the NINCDS–ADRDA criteria. Lancet Neurol 2007; 6: 734–46.

Dubois B, Feldman HH, Jacova C, Hampel H, Molinuevo JL, Blennow K, et al. Advancing research diagnostic criteria for Alzheimer's disease: the IWG-2 criteria. Lancet Neurol 2014; 13: 614–29.

Faul F, Erdfelder E, Buchner A, Lang AG. Statistical power analyses using G*Power 3.1: tests for correlation and regression analyses. Behav Res Methods 2009; 41: 1149–60.

Faul F, Erdfelder E, Lang AG, Buchner A. G*Power 3: a flexible statistical power analysis program for the social, behavioral, and biomedical sciences. Behav Res Methods 2007; 39: 175–91.

Finn ES, Scheinost D, Finn DM, Shen X, Papademetris X, Constable RT. Can brain state be manipulated to emphasize individual differences in functional connectivity? Neuroimage 2017; 160: 140–51.

Finn ES, Shen X, Scheinost D, Rosenberg MD, Huang J, Chun MM, et al. Functional connectome fingerprinting: identifying individuals using patterns of brain connectivity. Nat Neurosci 2015; 18: 1664.

Folstein MF, Folstein SE, McHugh PR. "Mini-mental state". A practical method for grading the cognitive state of patients for the clinician. J Psychiatr Res 1975; 12: 189–98.

Fonov V, Evans AC, Botteron K, Almli RC, McKinstry RC, Collins LD. Unbiased average age-appropriate atlases for pediatric studies. Neuroimage 2011; 54: 313–27.

Frisoni GB, Ganzola R, Canu E, Rüb U, Pizzini FB, Alessandrini F, et al. Mapping local hippocampal changes in Alzheimer's disease and normal ageing with MRI at 3 Tesla. Brain 2008; 131: 3266–76.

Gasbarri A, Packard MG, Campana E, Pacitti C. Anterograde and retrograde tracing of projections from the ventral tegmental area to the hippocampal formation in the rat. Brain Res Bull 1994; 33: 445–52.

Gonzalez-Castillo J, Handwerker DA, Robinson ME, Hoy CW, Buchanan LC, Saad ZS, et al. The spatial structure of resting state connectivity stability on the scale of minutes. Front Neurosci 2014; 8: 138.

Greene AS, Gao S, Scheinost D, Constable RT. Task-induced brain state manipulation improves prediction of individual traits. Nat Commun 2018; 9: 2807.

Grober E, Ocepek-Welikson K, Teresi JA. The free and cued selective reminding test: evidence of psychometric adequacy. Psychol Sci Q 2009; 51: 266–82.

Grothe MJ, Barthel H, Sepulcre J, Dyrba M, Sabri O, Teipel SJ, et al. In vivo staging of regional amyloid deposition. Neurology 2017; 89: 2031–8.

Hansson O, Seibyl J, Stomrud E, Zetterberg H, Trojanowski JQ, Bittner T, et al. CSF biomarkers of Alzheimer's disease concord with amyloid-β PET and predict clinical progression: a study of fully automated immunoassays in BioFINDER and ADNI cohorts. Alzheimers Dement 2018; 14: 1470–81.

Hoekert M, Kahn R, Pijnenborg M, Aleman A. Impaired recognition and expression of emotional prosody in schizophrenia: review and meta-analysis. Schizophr Res 2007; 96: 135–45.

Hogg RV, Tanis EA, Zimmerman DL. Probability and statistical inference. New York: Macmillan; 1977.

Hughes CP, Berg L, Danziger WL, Coben LA, Martin RL. A new clinical scale for the staging of dementia. Br J Psychiatry 1982; 140: 566–72.

Igloi K, Doeller CF, Paradis AL, Benchenane K, Berthoz A, Burgess N, et al. Interaction between hippocampus and cerebellum crus I in sequence-based but not place-based navigation. Cereb Cortex 2014; 25: 4146–54.

Jack CR, Bennett DA, Blennow K, Carrillo MC, Dunn B, Haeberlein SB, et al. NIA-AA Research Framework: toward a biological definition of Alzheimer's disease. Alzheimer's & Dementia 2018; 14: 535–62.

Jacobs H, Radua J, Lückmann HC. Meta-analysis of functional network alterations in Alzheimer's disease: toward a network biomarker. Neurosci Biobehav Rev 2013; 37: 753–65.

Janata P. The neural architecture of music-evoked autobiographical memories. Cereb Cortex 2009; 19: 2579–94.

Kang J, Namkoong K, Yoo S, Jhung K, Kim S. Abnormalities of emotional awareness and perception in patients with obsessive–compulsive disorder. J Affect Disord 2012; 141: 286–93.

Kim H. Neural activity that predicts subsequent memory and forgetting: a meta-analysis of 74 fMRI studies. Neuroimage 2011; 54: 2446–61.

Klein A, Andersson J, Ardekani BA, Ashburner J, Avants B, Chiang M-C, et al. Evaluation of 14 nonlinear deformation algorithms applied to human brain MRI registration. Neuroimage 2009; 46: 786–802.

Koelsch S, Skouras S. Functional centrality of amygdala, striatum and hypothalamus in a "small-world" network underlying joy: an fMRI study with music. Hum Brain Mapp 2014; 35: 3485–98.

Krokos E, Plaisant C, Varshney A. Virtual memory palaces: immersion aids recall. Virtual Real 2018; 22: 1–15.

Langville A, Meyer C. The mathematics of Google's PageRank, in Google's PageRank and beyond: the science of search engine rankings. Princeton, Oxford: Princeton University Press; 2006. pp. 31–46.

Leal SL, Landau SM, Bell RK, Jagust WJ. Hippocampal activation is associated with longitudinal amyloid accumulation and cognitive decline. Elife 2017; 6: e22978.

Lemieux L, Salek-Haddadi A, Lund TE, Laufs H. Modelling large motion events in fMRI studies of patients with epilepsy. Magn Reson Imaging 2007; 25: 894–901.

Leppänen J. Emotional information processing in mood disorders: a review of behavioral and neuroimaging findings. Curr Opin Psychiatry 2006; 19: 34–9.

Leutgeb S, Leutgeb JK, Treves A, Moser MB, Moser EI. Distinct ensemble codes in hippocampal areas CA3 and CA1. Science 2004; 305: 1295–8.

Lohmann G, Margulies DS, Horstmann A, Pleger B, Lepsien J, Goldhahn D, et al. Eigenvector centrality mapping for analyzing connectivity patterns in fMRI data of the human brain. PloS One 2010; 5: e10232.

Lohmann G, Müller K, Bosch V, Mentzel H, Hessler S. LIPSIA-Leipzig image processing and statistical inference algorithms. Technical report. Leipzig: Max-Planck-Institute of Cognitive Neuroscience; 2000.

Macinnes JJ, Dickerson KC, Chen N, Adcock RA. Cognitive neurostimulation: learning to volitionally sustain ventral tegmental area activation. Neuron 2016; 89: 1331–42.

Maddalena A, Papassotiropoulos A, Müller-Tillmanns B, Jung HH, Hegi T, Nitsch RM, Hock C. Biochemical diagnosis of Alzheimer disease by measuring the cerebrospinal fluid ratio of phosphorylated tau protein to β-amyloid peptide42. Arch Neurol 2003; 60: 1202–6.

Mannie Z, Bristow G, Harmer C, Cowen P. Impaired emotional categorisation in young people at increased familial risk of depression. Neuropsychologia 2007; 45: 2975–80.

Mizumori SJ, Ragozzino KE, Cooper BG, Leutgeb S. Hippocampal representational organization and spatial context. Hippocampus 1999; 9: 444–51.

Molinuevo JL, Gramunt N, Gispert JD, Fauria K, Esteller M, Minguillon C, et al. The ALFA project: a research platform to identify early pathophysiological features of Alzheimer's disease. Alzheimers Dement 2016; 2: 82–92.

Morris JC. The Clinical Dementia Rating (CDR): current version and scoring rules. Neurology 1993; 43: 2412–4.

Nicholson AA, Rabellino D, Densmore M, Frewen PA, Paret C, Kluetsch R, et al. The neurobiology of emotion regulation in posttraumatic stress disorder: amygdala downregulation via real-time fMRI neurofeedback. Hum Brain Mapp 2017; 38: 541–60.

Nobili A, Latagliata EC, Viscomi MT, Cavallucci V, Cutuli D, Giacovazzo G, et al. Dopamine neuronal loss contributes to memory and reward dysfunction in a model of Alzheimer's disease. Nat Commun 2017; 8: 14727.

Palmqvist S, Schöll M, Strandberg O, Mattsson N, Stomrud E, Zetterberg H, et al. Earliest accumulation of β-amyloid occurs within the default-mode network and concurrently affects brain connectivity. Nat Commun 2017; 8: 1214.

Penner MR, Mizumori S. Age-associated changes in the hippocampal-ventral striatum-ventral tegmental loop that impact learning, prediction, and context discrimination. Front Aging Neurosci 2012; 4: 22.

Pihlajamäki M, Sperling RA. fMRI: use in early Alzheimer's disease and in clinical trials. Future Neurol 2008; 3: 409–21.

Prince M, Wimo A, Guerchet M, Ali GC, Wu YT, Prina M, et al. The global impact of dementia: an analysis of prevalence, incidence, cost and trends. World Alzheimer Report. London: Alzheimer's Disease International; 2015.

Rami L, Valls-Pedret C, Bartres-Faz D, Caprile C, Sole-Padulles C, Castellvi M, et al. Cognitive reserve questionnaire. Values obtained in a healthy elderly population and in one with Alzheimer's disease. Rev Neurol 2011; 52: 195–201.

Reinhart R, Nguyen J. Working memory revived in older adults by synchronizing rhythmic brain circuits. Nat Neurosci 2019; 22: 820–7.

Reuter-Lorenz PA, Cappell KA. Neurocognitive aging and the compensation hypothesis. Curr Dir Psychol Sci 2008; 17: 177–82.

Schwindt GC, Black SE. Functional imaging studies of episodic memory in Alzheimer's disease: a quantitative meta-analysis. Neuroimage 2009; 45: 181–90.

Seeley WW, Crawford RK, Zhou J, Miller BL, Greicius MD. Neurodegenerative diseases target large-scale human brain networks. Neuron 2009; 62: 42–52.

Sitaram R, Ros T, Stoeckel L, Haller S, Scharnowski F, Lewis-Peacock J, et al. Closed-loop brain training: the science of neurofeedback. Nat Rev Neurosci 2017; 18: 86–100.

Skouras S, Scharnowski F. The effects of psychiatric history and age on self-regulation of the default mode network. NeuroImage 2019; 198: 150–9.

Skouras S, Falcon C, Tucholka A, Rami L, Sanchez-Valle R, Llado A, et al. Mechanisms of functional compensation, delineated by eigenvector centrality mapping, across the pathophysiological continuum of Alzheimer's disease NeuroImage. Clinical 2019a; 22: 101777.

Skouras S, Torner J, Anderson P, Koush Y, Falcon C, Minguillon C, et al. The effect of APOE genotype and streamline density volume, on hippocampal CA1 down-regulation: a real-time fMRI virtual reality neurofeedback study. bioRxiv 643577. 2019b; doi:10.1101/643577.

Smith SM, Fox PT, Miller KL, Glahn DC, Fox PM, Mackay CE, et al. Correspondence of the brain's functional architecture during activation and rest. Proc Natl Acad Sci USA 2009; 106: 13040–5.

Soares JM, Magalhães R, Moreira PS, Sousa A, Ganz E, Sampaio A, et al. A hitchhiker's guide to functional magnetic resonance imaging. Front Neurosci 2016; 10: 515.

Spreng RN, Grady CL. Patterns of brain activity supporting autobiographical memory, prospection, and theory of mind, and their

relationship to the default mode network. J Cogn Neurosci 2010; 22: 1112–23.

Stern Y, Gazes Y, Razlighi Q, Steffener J, Habeck C. A task-invariant cognitive reserve network. Neuroimage 2018; 178: 36–45.

Stoeckel LE, Garrison KA, Ghosh SS, Wighton P, Hanlon CA, Gilman JM, et al. Optimizing real time fMRI neurofeedback for therapeutic discovery and development. Neuroimage Clin 2014; 5: 245–55.

Strozyk D, Blennow K, White LR, Launer LJ. CSF Abeta 42 levels correlate with amyloid-neuropathology in a population-based autopsy study. Neurology 2003; 60: 652–6.

Tarvainen MP, Ranta-Aho PO, Karjalainen PA. An advanced detrending method with application to HRV analysis. IEEE Trans Biomed Eng 2002; 49: 172–5.

Teipel S, Drzezga A, Grothe MJ, Barthel H. Multimodal imaging in Alzheimer's disease: validity and usefulness for early detection. Lancet Neurol 2015; 14: 1037–53.

Torner J, Skouras S, Alpiste F, Gispert JD, Molinuevo JL. Multi-purpose virtual reality environment for biomedical applications. IEEE Trans Neural Syst Rehabil Eng 2019; 27: 1511–20.

Tran TT, Speck CL, Pisupati A, Gallagher M, Bakker A. Increased hippocampal activation in ApoE-4 carriers and non-carriers with amnestic mild cognitive impairment. Neuroimage Clin 2017; 13: 237–45.

Tustison NJ, Avants BB. Explicit B-spline regularization in diffeomorphic image registration. Front Neuroinform 2013; 7: 39.

Tustison N, Avants B, Cook P, Zheng Y, Egan A, Yushkevich P, et al. N4ITK: improved N3 bias correction. IEEE Trans Med Imaging 2010; 29: 1310–20.

Vazdarjanova A, Guzowski JF. Differences in hippocampal neuronal population responses to modifications of an environmental context: evidence for distinct, yet complementary, functions of CA3 and CA1 ensembles. J. Neurosci 2004; 24: 6489–96.

Wang H, Suh JW, Das SR, Pluta JB, Craige C, Yushkevich PA. Multi-atlas segmentation with joint label fusion. IEEE Trans Pattern Anal Mach Intell 2013; 35: 611–23.

Wechsler D. Escala de memoria de Wechsler – IV: manual técnico y de interpretación. Madrid: Pearson Educación; 2013.

Weiskopf N, Scharnowski F, Veit R, Goebel R, Birbaumer N, Mathiak K. Self-regulation of local brain activity using real-time functional magnetic resonance imaging (fMRI). J Physiol Paris 2004; 98: 357–73.

Wilson IA, Ikonen S, Gureviciene I, McMahan RW, Gallagher M, Eichenbaum H, et al. Cognitive aging and the hippocampus: how old rats represent new environments. J Neurosci 2004; 24: 3870–8.

Wink AM, de Munck JC, van der Werf YD, van den Heuvel OA, Barkhof F. Fast eigenvector centrality mapping of voxel-wise connectivity in functional magnetic resonance imaging: implementation, validation, and interpretation. Brain Connect 2012; 2: 265–74.

Yushkevich PA, Pluta JB, Wang H, Xie L, Ding SL, Gertje EC, et al. Automated volumetry and regional thickness analysis of hippocampal subfields and medial temporal cortical structures in mild cognitive impairment. Hum Brain Mapp 2015; 36: 258–87.